Korean Journal of Remote Sensing, Vol.33, No.1, 2017, pp.47~60
http://dx.doi.org/10.7780/kjrs.2017.33.1.5

ISSN 1225-6161 (Print)
ISSN 2287-9307 (Online)

Article

On the Spatial and Temporal Variability of L-band Polarimetric SAR Observations of Permafrost Environment in Central Yakutia

Sang-Eun Park* †

*Department of Energy and Mineral Resources Engineering, Sejong University

Abstract : The permafrost active layer plays an important role in permafrost dynamics. Ecological patterns, processes, and water and ice contents in the active layer are spatially and temporally complex depending on landscape heterogeneity and local-scale variations in hydrological processes. Although there has been emerging interest in the application of optical remote sensing techniques to permafrost environments, optical sensors are significantly limited in accessing information on near surface geo-cryological conditions. The primary objective of this study was to investigate capability of L-band SAR data for monitoring spatio-temporal variability of permafrost ecosystems and underlying soil conditions. This study exploits information from different polarimetric SAR observables in relation to permafrost environmental conditions. Experimental results show that each polarimetric radar observable conveys different information on permafrost environments. In the case of the dual-pol mode, the radar observables consist of two backscattering powers and one correlation coefficient between polarimetric channels. Among them, the dual-pol scattering powers are highly sensitive to freeze/thaw transition and can discriminate grasslands or ponds in thermokarst area from other permafrost ecosystems. However, it is difficult to identify the ground conditions with dual-pol observables. Additional backscattering powers and correlation coefficients obtained from quad-pol mode help understanding seasonal variations of radar scattering and assessing geo-cryological information on soil layers. In particular, co-pol coherences at HV-basis and circular-basis were found to be very useful tools for mapping and monitoring near surface soil properties.

Key Words : Synthetic aperture radar, dual-polarization, quad-polarization, microwave scattering mechanism, permafrost active layer, ALOS PALSAR.

1. Introduction

Permafrost is defined as soil, rock, and any other subsurface earth material that exists at or below 0°C for two or more consecutive years. Regions where permafrost underlies all or part of the ground surface occupy about 25% of land area in the Northern Hemisphere. There have been continues evidences to

Received February 13, 2017; Revised February 14, 2017, Accepted February 16, 2017.

† Corresponding Author: Sang-Eun Park (separk@sejong.ac.kr)

accumulate that climatic change is having a profound impact in the permafrost regions. Observations from global permafrost monitoring stations, such as the Thermal State of Permafrost (TSP) and the Circumpolar Active Layer Monitoring (CALM), indicate that there has been a general increase in permafrost temperatures during the last several decades across Alaska, northern Canada, Siberia, and northern Europe (Anisimov *et al*., 2001; Stocker *et al*., 2013).

The active layer, defined as the top layer of ground subject to annual thawing and freezing, plays an important role in permafrost dynamics because most ecological, hydrological, and geochemical activities take place within it (Brown 2000). However, there is widespread variation in water and ice contents in the active layer across a broad spectrum of spatial and temporal scales. Their seasonal and annual changes are spatially and temporally complex depending on many environmental factors, such as landscape heterogeneity and local hydrological processes. Consequently, in-situ measurements offer only limited insight into the impacts of global climate variations on the active layer dynamics. Radar remote sensing can be a useful observational tool for closing the gaps in permafrost monitoring with its ability to penetrate cloud and independence from solar illumination.

Most of previous studies on the application of radar remote sensing to permafrost environments have been particularly interested in the detection of landscape freeze/thaw states from variety of space-borne scatterometer and radiometer (Rignot and Way, 1994; Way *et al*., 1997; Frolking *et al*., 1999; Wisman, 2000; Kimball *et al*., 2001; Rawlins *et al*., 2005; Bartsch *et al*., 2007). There studies have shown that remotely-sensed freeze/thaw states can be useful for supporting ecologic and hydrological studies at regional, pan-boreal, and global scales (25~50km). In order to improve spatial resolution, Park *et al*. (2011) and Du *et al*., (2015) have used Synthetic Aperture Radar (SAR) data acquired at scanSAR mode for monitoring freeze/thaw process at moderate spatial resolution (1km~100m). However, there have been few studies on the application of high resolution SAR data to monitoring permafrost environments because of less data availability and increasing complexity in signals from heterogeneous permafrost landscape. Nonetheless, with an increasing availability of multi-frequency polarimetric space-borne SAR sensors, it is important to exploit full potential of the SAR remote sensing in the observation of spatially detailed information on permafrost dynamics.

This study aims to discuss the capability of L-band SAR data for monitoring spatio-temporal variability of permafrost ecosystems and underlying soil conditions in the active layer. The L-band PALSAR data of ALOS satellite over Eastern Siberia are used in this study to investigate the variations of scattering responses in permafrost ecosystems. In recent years, most of SAR systems including ALOS PALSAR have been operating several polarimetric modes: single-pol mode (HH or VV), dual-pol mode (HH/HV or VV/VH), and full or quad-pol mode (HH/HV/VH/VV). While the quad-pol data can provide several advantages in extracting physical quantities of the scattering targets, most of the SAR systems which have full polarization capability are often operated in dual-pol mode mainly because of the operational costs, such as power supply and coverage. This paper also discusses the utility and trade-off of dual-pol and quad-pol modes for monitoring arctic ecosystems and periglacial landforms.

2. SAR Measurements

1) Quad-pol data observables

In the imaging radar, a radiated electromagnetic wave is scattered by an object and one observes this wave. In general, the incident and scattered waves can

be completely described by the two-dimensional orthogonal basis (Lee and Pottier, 2009; Cloude, 2010). Then, one can consider the ground scatterer as a mathematical operator that takes one two-dimensional incident wave vector $\vec{E}^i$ and changes that into another scattered wave vector $\vec{E}^s$, which are related by the complex 2×2 scattering matrix [*S*], defined as:

$$\begin{bmatrix} E_H^s \\ E_V^s \end{bmatrix} = \begin{bmatrix} S_{HH} & S_{HV} \\ S_{VH} & S_{VV} \end{bmatrix} \begin{bmatrix} E_H^i \\ E_V^i \end{bmatrix} \quad (1)$$

where S_{pq} (q: polarization of the incident field; p: polarization of the scattered field) is the complex scattering amplitude which is dependent on the incidence angle, wavelength, and polarization of the radar system. For a given radar system, it is strongly related to the electrical and geometrical properties of the individual scatterers. Therefore, the complex scattering amplitudes of an object is the key measure of its scattering characteristics. The diagonal elements of the scattering matrix are called co-pol terms (the same polarization for the incident and the scattered fields). The off-diagonal elements are called cross-pol terms as they relate orthogonal polarization states. In addition, the total scattered power, called Span, is defined by the Frobenius norm (Span) of the scattering matrix, such as Span = $|S_{HH}|^2 + |S_{HV}|^2 + |S_{VH}|^2 + |S_{VV}|^2$.

In natural surfaces, the received wave in the SAR system is the coherent sum of the waves scattered from all individual scattering centers. Therefore, several measurements are often added to reduce statistical variations, such as the speckle filtering as well as the multi-look averaging. In this case, scattering properties of random media can be better described by the covariance matrix. In the monostatic backscattering case, where the transmitting and receiving antennas are placed at the same location, one can usually assume scattering reciprocity $S_{HV} = S_{VH}$. Then, the covariance matrix [C_3] can be formed by the complex scattering $\vec{k}_3 = [S_{HH}\ \sqrt{2}\,S_{HV}\ S_{VV})]^T$, such as

$$[C_3] = \langle \vec{k}_3 \vec{k}_3^{*T} \rangle = \begin{bmatrix} \langle S_{HH}S_{HH}^* \rangle & \sqrt{2}\langle S_{HH}S_{HV}^* \rangle & \langle S_{HH}S_{VV}^* \rangle \\ \sqrt{2}\langle S_{HV}S_{HH}^* \rangle & 2\langle S_{HV}S_{HV}^* \rangle & \sqrt{2}\langle S_{HV}S_{VV}^* \rangle \\ \langle S_{VV}S_{HH}^* \rangle & \sqrt{2}\langle S_{VV}S_{HV}^* \rangle & \langle S_{VV}S_{VV}^* \rangle \end{bmatrix} \quad (2)$$

where 〈 〉 represents the ensemble averaging and the superscript * denotes the complex conjugate. The multiplier $\sqrt{2}$ of S_{HV} is introduced to keep the norm (Span) of the scattering vectors.

Since the incoherently averaged [C_3] matrix is Hermitian, polarimetric observations are fully characterized by nine real parameters: three power terms and three complex correlation terms. Diagonal elements of the covariance matrix correspond to the multi-look scattering coefficients as

$$\begin{aligned} \sigma_{HH}^0 &= \langle S_{HH}S_{HH}^* \rangle = \langle |S_{HH}|^2 \rangle \\ \sigma_{HV}^0 &= \langle S_{HV}S_{HV}^* \rangle = \langle |S_{HV}|^2 \rangle \\ \sigma_{VV}^0 &= \langle S_{VV}S_{VV}^* \rangle = \langle |S_{VV}|^2 \rangle \end{aligned} \quad (3)$$

The co-pol scattering power terms have been widely studied in the literature, since all conventional space-borne SAR systems in 1990s were operated either HH or VV polarization mode. One the other hand, the cross-pol scattering power σ_{HV}^0 can be only obtained by polarimetric SAR systems in dual-pol or quad-pol mode. The cross-pol power is sensitive to the geometry of scattering surface and the presence of multiple or volume scattering (Oh *et al*., 1992; Lee *et al*., 2002; Lin *et al*., 2009).

Off-diagonal elements of the covariance matrix are complex cross product terms between polarizations. Without loss of generality, they can be described by the complex correlation coefficients between polarizations. The polarimetric correlation coefficient between XY and AB polarization channels is defined by

$$\gamma(XY, AB) = \frac{\langle S_{XY}S_{AB}^* \rangle}{\sqrt{\langle S_{XY}S_{XY}^* \rangle \langle S_{AB}S_{AB}^* \rangle}} = \rho_{XYAB} \exp(\phi_{XYAB}) \quad (4)$$

The co-pol and cross-pol products often contain little information in the case of natural distributed targets. In this case, called reflection symmetry, the correlation between co-pol and cross-pol channels, $\gamma(HH, HV)$ and $\gamma(HV, VV)$, are assumed to be zero. Nonzero

correlations between co- and cross-polarized components can be observed in case of the targets having a tilted local coordinate with respect to the radar coordinate, e.g., sloping terrain. Therefore, $\gamma(HH,HV)$ and $\gamma(HV,VV)$ can indicate the axis misalignment (Park *et al*., 2012). On the other hand, $\gamma(HH,VV)$ contains information on the scattering process. The magnitude of co-pol correlation (often called coherence) between HH and VV, ρ_{HHVV}, can be a good indicator of signal depolarization. It will be zero for a completely random signal and one for a pure polarized signal. High ρ_{HHVV} values can be found in the single surface scattering case, while multiple or volume scattering results in low ρ_{HHVV} values (Park *et al*., 2013; Chowdhury *et al*., 2014).

2) Dual-pol data observables

Space-borne SAR instruments often employ a single transmitted polarization state and a coherent dual channel receiver giving rise to dual-pol data. Dual-pol radars are not capable of reconstructing the complete scattering matrix in equation (1), but instead can be used to reconstruct a column of [*S*] matrix. In the case of H-pol transmission, the basic scattering measurement of a pixel becomes

$$\vec{k}_{2h} = \begin{bmatrix} S_{HH} & S_{HV} \\ S_{VH} & S_{VV} \end{bmatrix} \begin{bmatrix} 1 \\ 0 \end{bmatrix} = \begin{bmatrix} S_{HH} \\ S_{VH} \end{bmatrix}. \quad (5)$$

The resulting dual-pol covariance matrix after multi-look processing is given by

$$[C_{2h}] = \langle \vec{k}_{2h}\, \vec{k}_{2h}^{*T} \rangle = \begin{bmatrix} \langle |S_{HH}|^2 \rangle & \langle S_{HH} S_{VH}^* \rangle \\ \langle S_{VH} S_{HH}^* \rangle & \langle |S_{VH}|^2 \rangle \end{bmatrix}. \quad (6)$$

Consequently, the dual-pol data provides only two scattering powers and one correlation coefficient between co- and cross-polarized scattering amplitudes. If the terrain exhibits reflection symmetry (a common case in microwave remote sensing of natural surface), the off-diagonal term in $[C_{2h}]$ will be zero: $\langle S_{HH} S_{VH}^* \rangle = 0$, and there will be only two observables. If we transmit V-pol signal only and receive both, the similar considerations can be applied with minor modification. In this case, the covariance matrix becomes

$$[C_{2v}] = \begin{bmatrix} \langle |S_{HV}|^2 \rangle & \langle S_{HV} S_{VV}^* \rangle \\ \langle S_{VV} S_{HV}^* \rangle & \langle |S_{VV}|^2 \rangle \end{bmatrix}. \quad (7)$$

3. SAR Data Analysis

1) Study sites and data set

The selected study site is located in alluvial terrain of Lena River near Yakutsk, eastern Siberia (Fig. 1). It has relatively flat topography and is underlain by continuous permafrost. Average monthly temperatures in this region range from 19 ˚C in July to -40 ˚C in January. The permafrost front reached the surface during winter, and the active layer depth in the growing season could be about 1-3 m (Brouchkov *et al*., 2004; Lopez *et al*., 2007; Iijima *et al*., 2010).

Three ALOS PALSAR quad-pol mode data were acquired over heterogeneous forest and grass surfaces on the left and right banks of Lena River (Fig. 1). The data set covered a freeze/thaw cycle from November 2006 to May 2007. According to the meteorological data obtained from the nearest grid point of global atmospheric reanalysis product (Dee *et al*., 2011), air temperature changed significantly from frozen condition in November and March to thawed conditions in May (Table 1).

The study site covered with pure and mixed forests, shrublands, and thermokarst landforms. Particularly, one of distinct features of the central Yakutia is the abundance of thermokarst depressions called “alases”, which ranges from several meters to more than 20 m in depth (Brouchkov *et al*., 2004; Lopez *et al*., 2007; Iijima *et al*., 2010). It is developed in response of the thawing of upper part of ice rich permafrost leading to the formation of depression. Central Yakutia area is well suited to thermokarst because the alluvial terraces of Lena River consist of silty and sandy loams with high ice contents. Alases are usually covered by either

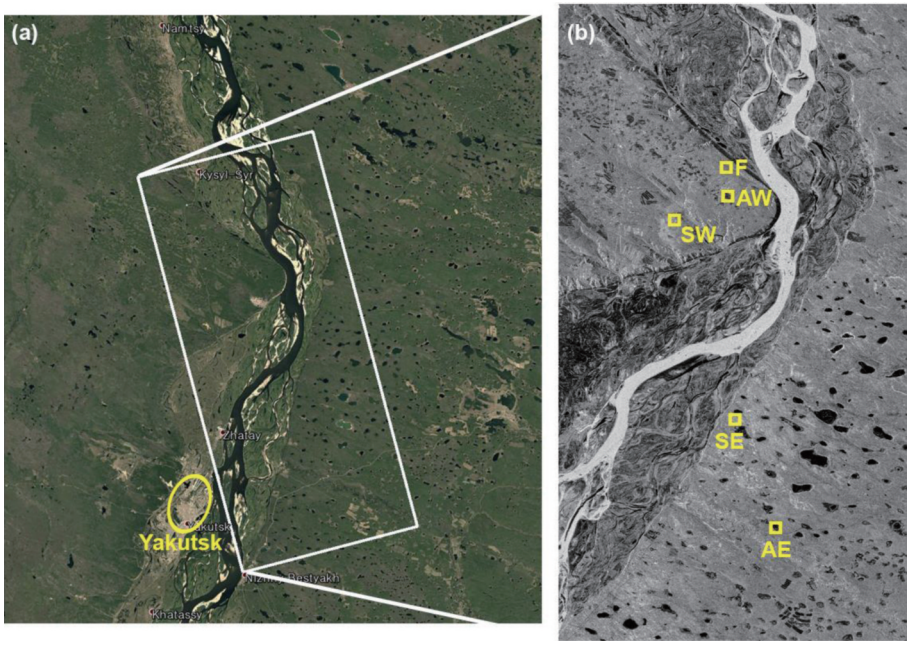

Fig. 1. (a) Location of the study site and SAR data coverage marked on the Google Earth optical image. (b) An example of acquired ALOS PALSAR image (σ^0_{HH}) and five test sites (F, SW, SE, AW, AE) selected in this study (see Section 3.1).

Table 1. PALSAR data acquisition

Polarization	Date	Incidence angle	Air temperature	Top soil temperature	Snow water equivalent
Quad-pol	2006/11/03	23.8˚	-21.4˚C	-14.0˚C	0.04 m
Quad-pol	2007/03/21	23.8˚	-10.7˚C	-24.9˚C	0.14 m
Quad-pol	2007/05/06	23.9˚	6.4˚C	1.9˚C	0 m

grassland with or without small ponds or sizeable lakes.

It should be noted that a number of alas patches exist on the right (East) bank of Lena River as one can identify from the optical and SAR images (Fig. 1). In addition, one can identify a distinctive elevation difference between left bank uplands and right bank lowlands (see Fig. 4(d)). Consequently, there could be substantial differences in the soil properties, such as water and ice content, permeability, and salinity, between the left and right banks of Lena River (Hiyama *et al*., 2003; Grosse and Jones, 2011). In this context, five test sites were manually selected for the analysis of SAR scattering responses as in indicated in Fig. 1. The selected test areas consist of forested areas (F1), shrublands in the left (SW) and right (SE) banks, and isolated grassland in alas region in the left (AW) and right banks (AE) of Lena River.

2) Dual-pol radar response

According to the observation strategy, ALOS PALSAR acquired polarimetric data primarily in the fine-beam dual-pol mode (single polarization transmission and dual coherent reception). The dual-pol covariance matrix data provides two scattering powers and one co-pol and cross-pol correlation. In this study, the quad-pol mode data are used to simulate dual-pol mode data by using equations (5) and (6).

Fig. 2 shows seasonal variations of σ^0_{HH} and σ^0_{HV} (here, HV denotes H-pol transmission and V-pol reception) over the study site. In both polarimetric channels, drastic seasonal changes with thawing are easily observed across all landscapes. Under frozen conditions, both σ^0_{HH} and σ^0_{HV} show low values in most

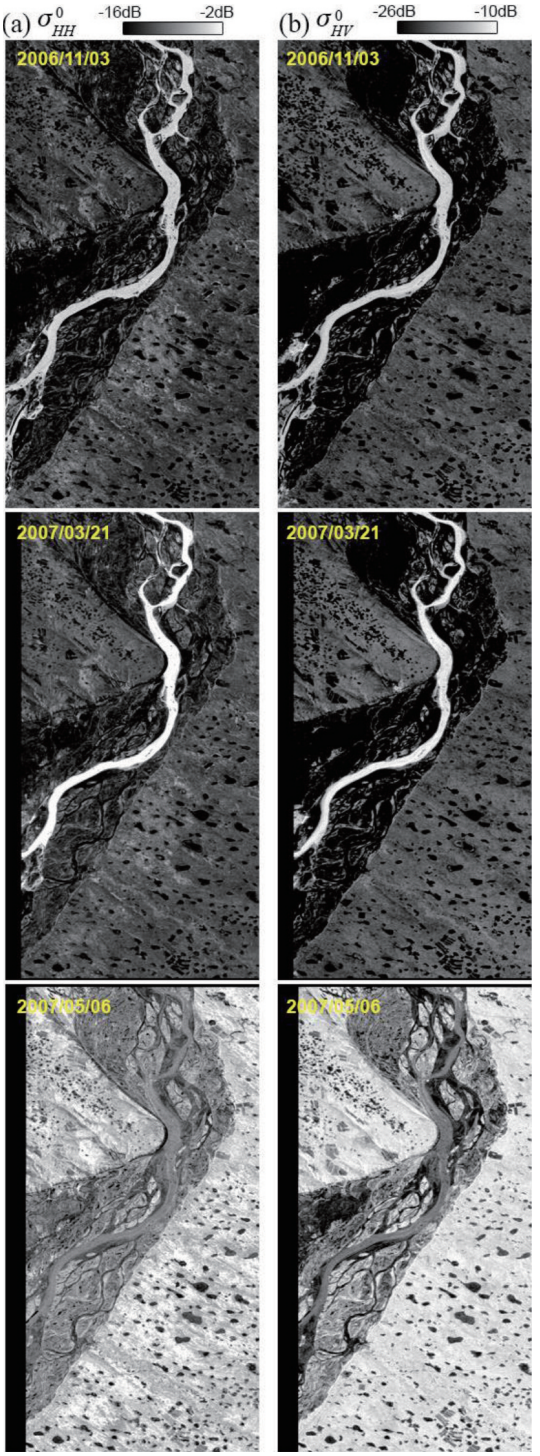

Fig. 2. Seasonal variations of PALSAR dual-pol scattering powers at (a) HH and (b) HV polarimetric channels.

areas except river ice. The scattering powers in the frozen river are comparable to those in vegetated areas

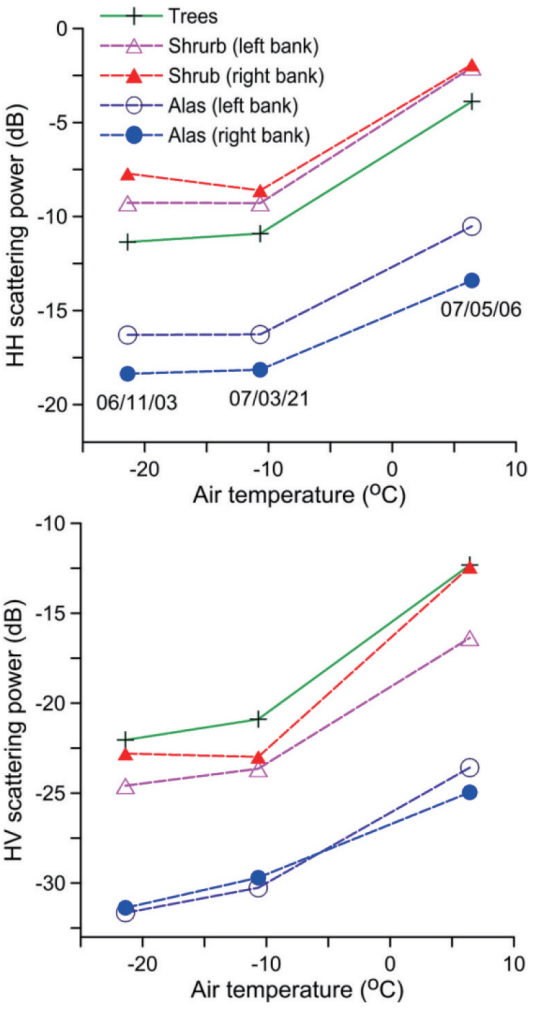

Fig. 3. Seasonal variations of mean scattering powers σ^0_{HH} and σ^0_{HV} in five test areas.

observed at thawed condition. Both surface and volume scattering mechanisms in consolidated ice can be related to such scattering behavior in river ice. There have been several studies on monitoring river ice with SAR remote sensing (Mermoz *et al*., 2009; Gauthier *et al*., 2010; Mermoz *et al*., 2014). However this study will stay focused on the land surface dynamics. In land surface, scattering powers are increased significantly with thawing primarily due to increases of the dielectric constant of the scattering media.

Fig. 3 further illustrates how the backscattering powers at frozen and thawed states vary with permafrost landscape especially in five test areas. It is

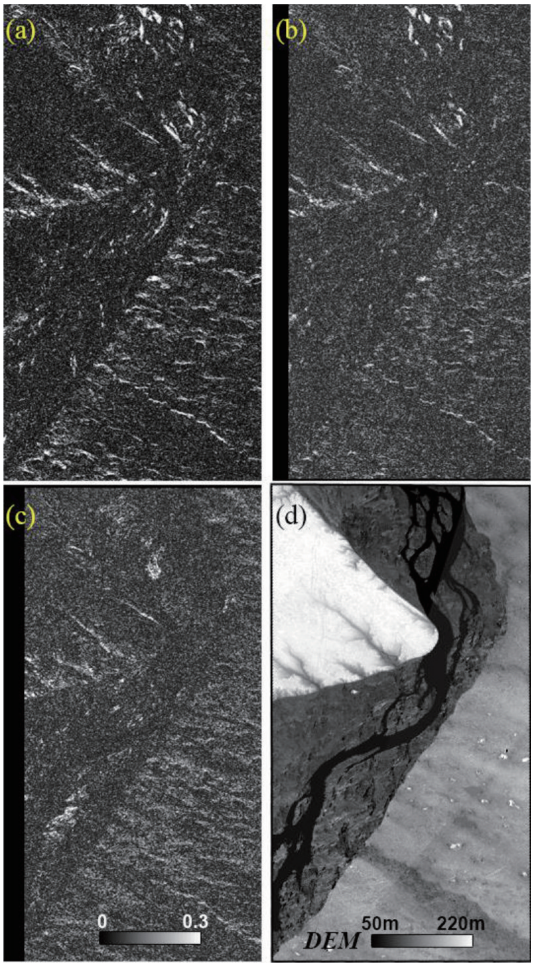

Fig. 4. PALSAR dual-pol correlation coefficient ρ_{HHHV} images acquired on (a) 2006/11/03(frozen), (b) 2007/03/21 (frozen), and (c) 2007/05/06 (thawed). For comparison, ASTER GDEM (Global Digital Elevation Model) over the study site is also shown in (d).

shown that (1) both σ^0_{HH} and σ^0_{HV} show high temporal consistency under frozen conditions, (2) σ^0_{HV} is more sensitive than σ^0_{HH} to freeze/thaw transition, (3) temporal trends of scattering powers have little dependency on land cover types, (4) both σ^0_{HH} and σ^0_{HV} can be useful to distinguish shrublands and grasslands, (5) differences in cryological characteristics between the left and right banks are hardly distinguishable in the dual-pol scattering powers.

Fig. 4 shows remaining off-diagonal element in the dual-pol covariance matrix, i.e., co-pol and cross-pol correlation. As discussed above, the magnitudes of correlation ρ_{HHHV} acquired at frozen and thawed conditions are close to zero across the study site regardless of extreme seasonal changes in the dielectric properties. By comparing ρ_{HHHV} to the digital surface model obtained from ASTER GDEM (Global Digital Elevation Model) product (Abrams *et al*., 2010) in Fig. 4(d), nonzero ρ_{HHHV} values are highly related to the terrain slopes. Consequently, it can be a useful parameter to augment mapping large scale relief structures or geomorphological features in permafrost areas.

3) Quad-pol radar response

The quad-pol covariance matrix under reflection symmetry can provide one additional scattering power term σ^0_{HH} and another correlation term ρ_{HHVV}. Fig. 5 shows seasonal variations of σ^0_{VV} and ρ_{HHVV} over the study site. Seasonal variations of σ^0_{VV} follow similar temporal patterns to σ^0_{HH} but exhibit less sensitivity to freeze-thaw transition of the permafrost ecosystem. On the other hand, spatial and temporal patterns of ρ_{HHVV} are quite distinct from those in other polarimetric parameters. Unlike the backscattering intensities, one can clearly identify changes in ρ_{HHVV} values between the beginning and the end of the freezing seasons.

Fig. 6 shows spatial and temporal patterns of ρ_{HHVV} in five test areas. Significant decreases in ρ_{HHVV} values between the beginning and the end of the freezing seasons can be identified in all test areas. In the beginning of the freezing season, some parts of soil layers can be in thawed conditions while most soil media and organic layer are in frozen conditions in the end of the freezing season. Therefore, it is possible to assume that dielectric properties of the active layer are different in the beginning and end of the freezing seasons. This can cause a drop in ρ_{HHVV} since dielectric discontinuities distributed through a soil media affect the signal depolarization. In addition, as discussed in Section 3.1, water and ice contents can be different in the left and right banks. Consequently, ρ_{HHVV} values

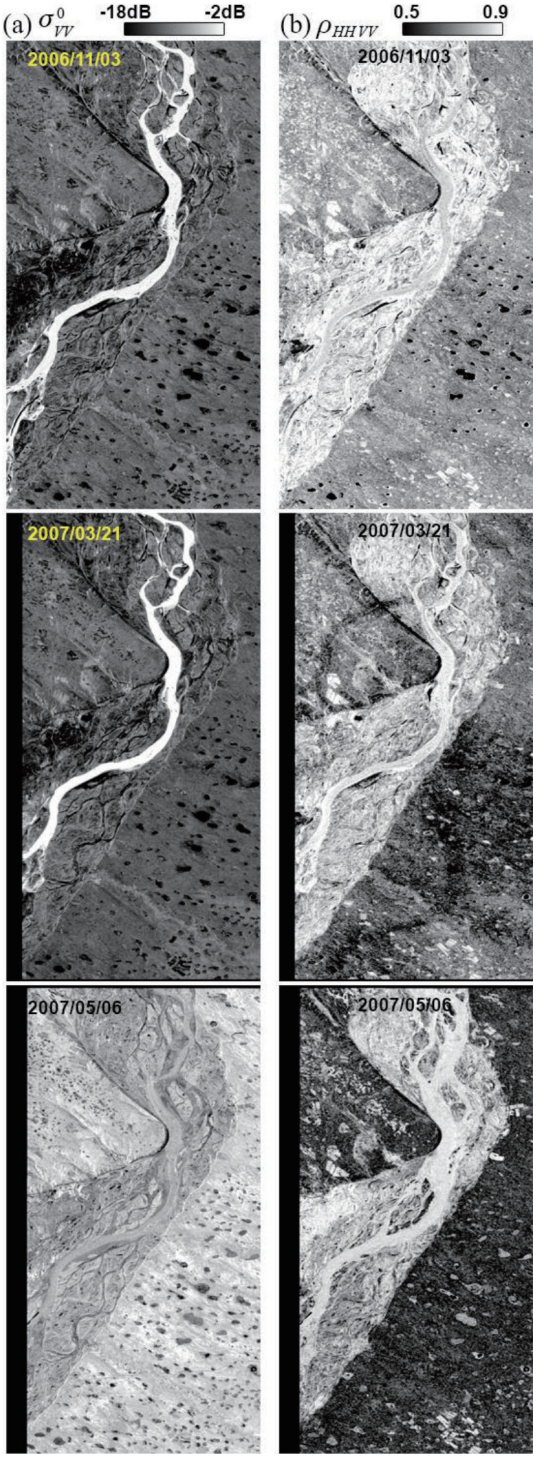

Fig. 5. Seasonal variations of (a) VV-pol scattering power (σ^0_{VV}) and (b) correlation between HH and VV polarimetric channels (ρ_{HHVV}).

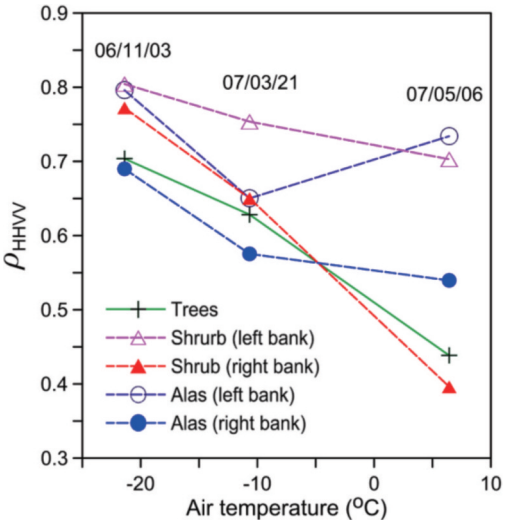

Fig. 6. Seasonal variations of mean ρ_{HHVV} values in five test areas.

observed the left and right banks also show significant differences from each other. It is shown that ρ_{HHVV} values in the alluvial lowlands (right bank) are lower than those in the left bank.

One of the main advantages of quad-pol SAR observation is the fact that once a scattering response is acquired in one polarization basis (e.g., HV-basis), it can be represented in any other polarimetric basis by a simple mathematical transformation (Boerner *et al.*, 1981, Lee and Pottier, 2009). Therefore, it is possible to reconstruct SAR observables different from the usual H or V polarization state.

Among the infinite possible combinations of transmitting and receiving polarizations, an important special case is the form of the scattering matrix in the right (R) and left (L) handed circular polarization basis [S_c]. It can be obtained by a unitary transformation of the linear [S] matrix as

$$[S_c]=\begin{bmatrix}S_{RR} & S_{RL}\\ S_{LR} & S_{LL}\end{bmatrix}=\frac{1}{2}\begin{bmatrix}1 & i\\ i & 1\end{bmatrix}\begin{bmatrix}S_{HH} & S_{HV}\\ S_{VH} & S_{VV}\end{bmatrix}\begin{bmatrix}1 & i\\ i & 1\end{bmatrix}$$
$$\frac{1}{2}\begin{bmatrix}S_{HH}-S_{VV}+2iS_{HV} & i(S_{HH}+S_{VV})\\ i(S_{HH}+S_{VV}) & S_{VV}-S_{HH}+2iS_{HV}\end{bmatrix} \quad (8)$$

By defining a circular basis $\vec{k}_{3c}=[(S_{RR}\sqrt{2}\,S_{RL}\,S_{LL})]^T$, one can derive multi-look circular polarization

covariance matrix as

$$[C_{3c}] = \langle \vec{k}_{3c} \vec{k}_{3c}^{*T} \rangle = \begin{bmatrix} \langle S_{RR} S_{RR}^* \rangle & \sqrt{2}\langle S_{RR} S_{RL}^* \rangle & \langle S_{RR} S_{LL}^* \rangle \\ \sqrt{2}\langle S_{RL} S_{RR}^* \rangle & 2\langle S_{RL} S_{RL}^* \rangle & \sqrt{2}\langle S_{RL} S_{LL}^* \rangle \\ \langle S_{LL} S_{RR}^* \rangle & \sqrt{2}\langle S_{LL} S_{RL}^* \rangle & \langle S_{LL} S_{LL}^* \rangle \end{bmatrix} \quad (9)$$

The circular polarization basis has been providing a good platform for planetary radar and terrestrial radar at longer wavelengths, which can be subject to significant Faraday rotation as they pass through the ionosphere. The circular polarization covariance matrix provides additional three scattering powers and three complex correlation coefficients between right and left handed circular polarizations. Among them, the correlation between the RR and LL circular polarizations $\gamma(RR, LL)$ has been actively studied in the radar remote sensing of Earth observation.

Unlike to ρ_{HHVV}, the magnitude of circular polarization correlation ρ_{RRLL} can be lower in both the single surface scattering and depolarized volume scattering mechanisms. A high degree of coherence between RR and LL rather indicates a dominance of double-bounce scattering, which can be used for mapping man-made structures (Moriyama *et al*., 2005, Yamaguchi *et al*., 2008). In addition, ρ_{RRLL} has been found very sensitive to the roughness of scattering surfaces (Mattia *et al*., 1997; Park *et al*., 2009). Furthermore, the phase of circular polarization correlation ϕ_{RRLL} has been found to be directly related to the local orientation angle of scattering surface induced by the local topography (Lee *et al*., 2002).

Fig. 7 shows seasonal variations of ρ_{RRLL} and ϕ_{RRLL} of the study site. It is shown several distinctive features that (1) both ρ_{RRLL} and ϕ_{RRLL} are much less sensitive to freeze/thaw transition than other radar observables, (2) ρ_{RRLL} values obtained at both frozen and thawed conditions exhibit distinctive spatial patterns allowing discrimination of cryological characteristics between the left and right banks, and (3) ϕ_{RRLL} is sensitive not to the permafrost ecosystem or soil condition but to the terrain slope. This relationship is most obvious at frozen condition.

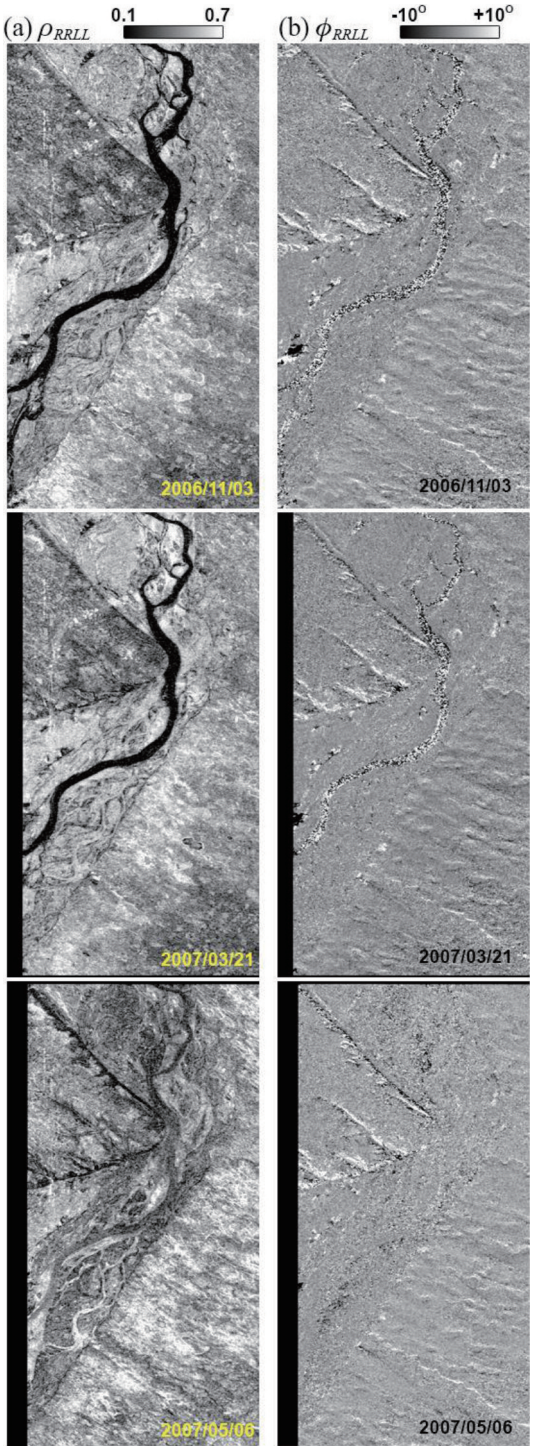

Fig. 7. Seasonal variations of (a) the magnitude ρ_{RRLL} and (b) the phase ϕ_{RRLL} of circular polarization correlation.

Fig. 8 shows spatial variability of ρ_{RRLL} in five test areas. Note that, in order to better reflect inherent

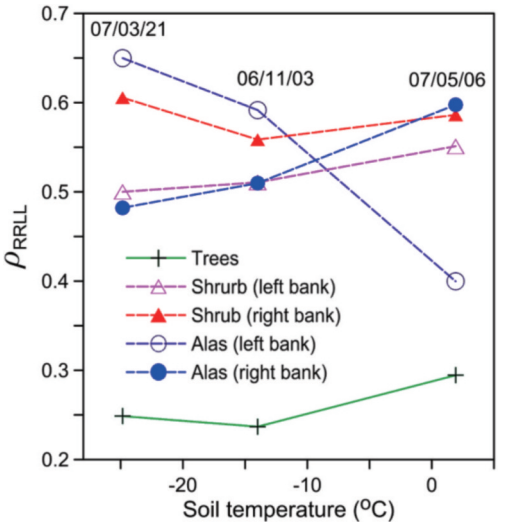

Fig. 8. Seasonal variations of mean ρ_{RRLL} values in five test areas.

temporal trends of ρ_{RRLL}, the mean ρ_{RRLL} values in test areas are plotted as a function of soil temperature from nearest weather station (Table 1). ρ_{RRLL} provides enhanced contrast between the left and right banks. As discussed above, distinctive differences in the terrain elevation and the thermokarst lake distribution between the left and right bank of Lena River can be identified. Therefore, there could be substantial differences in the ground hydrological condition between the left and right banks. Maximum differences in ρ_{RRLL} values between the opposite sides of Lena River are observed when the ground layers are fully frozen (minimum soil temperature). Therefore, although physical causal mechanisms about these characteristic scattering properties cannot be confirmed at this stage, ρ_{RRLL} can probably be related to local cryogenic processes, e.g., frost heave, occurring on the scattering surface.

Fig. 9 shows closer look of polarimetric parameters in the left and right banks of Lena River observed in the end of freezing season (2007/03/21). Alas areas (covered with grass or lake) on both sides are clearly distinguishable from neighboring shrublands by the HV-pol scattering power represented in the first row. Spatial patterns of the co-pol coherences ρ_{RRLL} and ρ_{RRLL} in the second row are not only varied with the land cover types but also affected by the ground conditions. Despite of similarities in land cover types, coherence

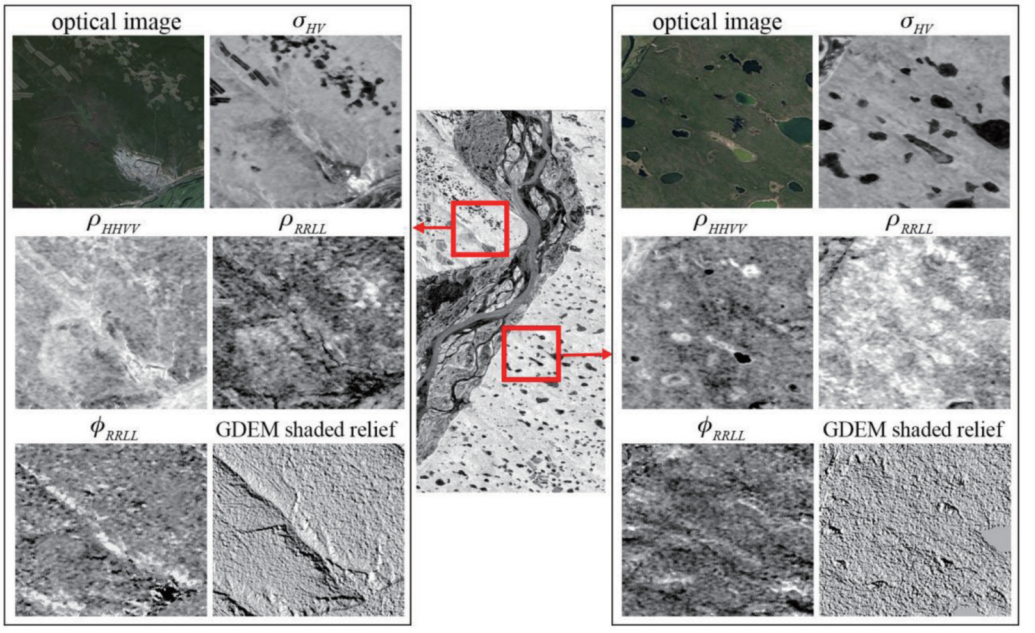

Fig. 9. Closer look of polarimetric parameters in the left bank (left panel) and the right bank (right panel) of Lena River observed on 2007/03/21. For comparison, high resolution optical images from the Google Earth and shaded relief images derived from the ASTER GDEM are also shown in this figure.

levels between the left bank uplands and right bank lowlands are distinguishable from each other.

On the other hand, spatial patterns of ϕ_{RRLL} exhibit no relationship with either land cover types or soil conditions. By compared to the DEM derived shaded relief map on the left panel of Fig. 9, ϕ_{RRLL} is closely correspondent with the surface slope. In addition, as shown on the right panel of Fig. 9, characteristic surface depressions in thermokarst areas can be clearly identified in the ϕ_{RRLL} image, while they are not detectable in ASTER GDEM. This is particularly important in permafrost monitoring because most periglacial processes are related to local relief and geomorphological characteristics, e.g., patterned ground, hummocks, palsas, pingos, and thermokarst.

4. Conclusions

With the remoteness and vast distribution of permafrost, there has been emerging interest in the application of remote sensing techniques to observe and monitor permafrost environments. Space-borne and air-borne optical sensors have been widely used for remote sensing of permafrost landscapes for several decades. However, optical sensors are significantly limited in accessing information on near surface geo-cryological conditions which play an important role in permafrost dynamics. In this context, low frequency active microwave sensors can be particularly valuable in permafrost observation.

The primary objective of this study was to investigate capability of L-band SAR data for monitoring permafrost ecosystems and underlying soil conditions. Particularly, this study presented spatial and temporal behaviors of SAR signals subject to seasonal cryogenic activities from the beginning of freezing season to the beginning of melting season. This study also placed focus on exploiting information from different polarimetric SAR observables in relation to environmental conditions. Central Yakutia area investigated in this study is a well-known example of thermokarst terrain. Thermokarst formation process is typical within areas of degrading ice rich permafrost resulting in a localized depression. Since development of thermokarst affects local hydrology, biota, and biogeochemical processes, the study site can be a good example highlights the importance of the volume and the morphology of the ground ice distribution.

The experimental results presented show that each polarimetric radar observable conveys different information on the scattering surface. In the case of the dual-pol mode with H-pol transmission, the radar observables consist of two backscattering powers (σ^0_{HH} and σ^0_{HV}) and one correlation coefficient between co-pol and cross-pol channels (ρ_{HHHV}). Although ρ_{HHHV} provides no information for reflection symmetric media, σ^0_{HH} and σ^0_{HV} are highly sensitive to freeze/thaw transition and can discriminate grasslands or ponds in thermokarst area from other permafrost ecosystems. However, it is difficult to identify the ground conditions with dual-pol observables.

A complete polarimetric scattering matrix can be obtained from quad-pol mode. Additional backscattering powers and correlation coefficients between polarimetric channels help understanding seasonal variations of radar scattering and assessing geo-cryological information on soil layers. In particular, co-pol coherences at HV-basis and circular-basis were found to be very useful tools for mapping and monitoring land cover types and near surface soil properties in the permafrost active layer, such as water and ice contents, geomorphic features, and periglacial activities.

One of the main limitations of this study is the lack of reference information. The availability of in-situ data is restricted because of sparse measurement stations, limited data accessibility, and a lack of regional details in the documentation. The physical model-based prediction of polarimetric signals as well as other

independent data, e.g., multi-frequency radar, will be helpful to partly overcome this problem and to design retrieval algorithm for permafrost variables.

Acknowledgment

The author is grateful to JAXA for providing ALOS PALSAR data. This work was supported by MSIP (Ministry of Science, ICT & Future Planning, Korea), under Basic Science Research Program (2015R1C1 A1A02037584) through the National Research Foundation of Korea and under ITRC (Information Technology Research Center) support Program (IITP-2016-R2718-16-0014) through the National IT Industry Promotion Agency.

References

Abrams, M., B. Bailey, H. Tsu, and M. Hato, 2010. The ASTER Global DEM, *Photogrammetric Engineering and Remote Sensing*, 76(4):344-348.

Anisimov, O., B. Fitzharris, J.O. Hagen, R. Jeffries, H. Marchant, F.E. Nelson, T. Prowse, and D.G. Vaughan, 2001. *Polar Regions (Arctic and Antarctic): Climate Change: Impacts, Adaptation, and Vulnerability, the Contribution of Working Group II of the Intergovernmental Panel on Climate Change, Third Assessment Review*, Cambridge University Press, Cambridge UK.

Bartsch, A., R. Kidd, W. Wagner, and Z. Bartalis, 2007. Temporal and spatial variability of the beginning and end of daily spring freeze/thaw cycles derived from scatterometer data, *Remote Sensing of Environment*, 106(3): 360-374.

Boerner, W.-M., M.B. El-Arini, C.-Y. Chan, P.M. Mastoris, 1981. Polarization dependence in electromagnetic inverse problems, *IEEE Transactions on Antennas and Propagation*, AP-29(2):162-271.

Brouchkov, A., M. Fukuda, A. Fedorov, P. Konstantinov, and G. Iwahana, 2004. Thermokarst as a short-term permafrost disturbance, Central Yakutia, *Permafrost and Periglacial Processes*, 15(1): 81-87.

Brown, J., K.M. Hinkel, and F.E. Nelson, 2000. The circumpolar active layer monitoring (CALM) program: research designs and initial results, *Polar Geography*, 24(3): 166-258.

Chowdhury, T.A., C. Thiel, C. Schmullius, 2014. Growing stock volume estimation from L-band ALOS PALSAR polarimetric coherence in Siberian forest, *Remote Sensing of Environment*, 155: 129-144.

Cloude, S.R., 2010. *Polarisation: Applications in Remote Sensing*, Oxford University Press, Oxford, UK.

Dee, D.P, S.M. Uppala, A.J. Simmons, P. Berrisford, P. Poli, S. Kobayashi, U. Andrae, M.A. Balmaseda, G. Balsamo, P. Bauer, P. Bechtold, A.C.M. Beljaars, L. van de Berg, J. Bidlot, N. Bormann, C. Delsol, R. Dragani, M. Fuentes, A.J. Geer, L. Haimberger, S.B. Healy, H. Hersbach, E.V. Hólm, L. Isaksen, P. Kållberg, M. Köhler, M. Matricardi, A.P. McNally, B.M. Monge-Sanz, J.-J. Morcrette, B.-K. Park, C. Peubey, P. de Rosnay, C. Tavolato, J.-N. Thépaut, and F. Vitart, 2011. The ERA-Interim reanalysis: Configuration and performance of the data assimilation system, *Quarterly Journal of the Royal Meteorological Society*, 137(656): 553-597.

Du, J., J.S. Kimball, M. Azarderakhsh, R.S. Dunbar, M. Moghaddam, K.C. McDonald, 2015. Classification of Alaska Spring Thaw Characteristics Using Satellite L-Band Radar Remote Sensing, *IEEE Transactions on*

Geoscience and Remote Sensing, 53(1): 542-556.

Frolking, S., K.C. McDonald, J.S. Kimball, J.B. Way, R. Zimmermann, and S.W. Running, 1999. Using the space-borne NASA scatterometer (NSCAT) to determine the frozen and thawed seasons of a boreal landscape, *Journal of Geophysical Research*, 104(D22): 27895-27908.

Gauthier, Y., M. Tremblay, M. Bernier, and C. Furgal, 2010. Adaptation of a radar-based river ice mapping technology to the Nunavik context, *Canadian Journal of Remote Sensing*, 36: 168-185.

Grosse, G. and B.M. Jones, 2011. Spatial distribution of pingos in northern Asia, *Cryosphere*, 5(1):13-33.

Hiyama, T., M.A. Strunin, R. Suzuki, J. Asanuma, M.Y. Mezrin, N.A. Bezrukova, and T. Ohata, 2003. Aircraft observations of the atmospheric boundary layer over a heterogeneous surface in eastern Siberia, *Hydrological Processes*, 17(14): 2885-2911.

Iijima, Y., A.N. Fedorov, H. Park, K. Suzuki, H. Yabuki, T.C. Maximov, and T. Ohata, 2010. Abrupt increases in soil temperatures following increased precipitation in a permafrost region, Central Lena River Basin, Russia, *Permafrost and Periglacial Processes*, 21(1): 30-41.

Kimball, J. S., K.C. McDonald, A.R. Keyser, S. Frolking, and S.W. Running, 2001. Application of the NASA scatterometer (NSCAT) for determining the daily frozen and nonfrozen landscape of Alaska, *Remote Sensing of Environment*, 75(1): 113-126.

Lee, J.S. and E. Pottier, 2009. *Polarimetric Radar Imaging: From Basics to Applications*, CRC Press, Boca Raton, Fla, USA.

Lee, J.S., D.L. Schuler, T.L. Ainsworth, E. Krogager, D. Kasilingam, and W.M. Boerner, 2002. On the estimation of radar polarization orientation shifts induced by terrain slopes, *IEEE Transactions on Geoscience and Remote Sensing*, 40(1): 30-41.

Lin, H., J. Chen, Z. Pei, S. Zhang, and X. Hu, 2009. Monitoring sugarcane growth using ENVISAT ASAR data, *IEEE Transactions on Geoscience and Remote Sensing*, 47(8): 2572-2580.

Lopez, C.M.L., A. Brouchkov, A. Nakayama, F. Takakai, AN.N. Fedorov, and M. Fukuda, 2007. Epigenetic salt accumulation and water movement in the active layer of central Yakutia in eastern Siberia, *Hydrological Processes*, 21(1):103-109.

Mattia, F., T. Le Toan, J.C. Souyris, G. De Carolis, N. Floury, F. Posa, and G. Pasquariello, 1997. The effect of surface roughness on multifrequency polarimetric SAR data, *IEEE Transaction on Geoscience and Remote Sensing*, 35(4): 954-965.

Mermoz, S., S. Allain, M. Bernier, E. Pottier, J.J. Van Der Sanden, and K. Chokmani, 2014. Retrieval of river ice thickness from C-Band PolSAR data, *IEEE Transaction on Geoscience and Remote Sensing*, 52(6):3052-3062.

Mermoz, S., S. Allain, M. Bernier, E. Pottier, and I. Gherboudj, 2009. Classification of river ice using polarimetric SAR data, *Canadian Journal of Remote Sensing*, 35(5):460-473.

Moriyama, T., Y. Yamaguchi, S. Uratsuka, T. Umehara, H. Maeno, M. Satake, A. Nadai, and K. Nakamura, 2005. A study on polarimetric correlation coefficient for feature extraction of polarimetric SAR data, *IEICE Transactions on Communications*, 88(6): 2355-2361.

Oh, Y., K. Sarabandi, and F.T. Ulaby, 1992. An empirical model and an inversion technique for radar scattering from bare soil surfaces, *IEEE Transactions on Geoscience and Remote Sensing*, 30(2): 370-381.

Park, S.-E., Y. Yamaguchi, and D. Kim, 2013. Polarimetric SAR remote sensing of the 2011 Tohoku earthquake using ALOS/PALSAR, *Remote Sensing of Environment*, 132: 212-220.

Park, S.-E., W.M. Moon, and E. Pottier, 2012. Assessment of scattering mechanism of polarimetric SAR signal from mountainous forest areas, *IEEE Transaction on Geoscience and Remote Sensing*, 50(11): 4711-4719.

Park, S.-E., A. Bartsch, D. Sabel, W. Wagner, V. Naeimi, and Y. Yamaguchi, 2011. Monitoring freeze/thaw cycles using ENVISAT ASAR global mode, *Remote Sensing of Environment*, 115(12): 3457-3467.

Park, S.-E., W.M. Moon, D. Kim, and J.-E. Kim, 2009. Estimation of surface roughness parameter in intertidal mudflat using airborne polarimetric SAR data, *IEEE Transaction on Geoscience and Remote Sensing*, 47(4): 1022-1031.

Rawlins, M.A, K.C. McDonald, S. Frolking, R.B. Lammers, M. Fahnestock, J.S. Kimball, and C.J. Vorosmarty, 2005. Remote Sensing of Pan-Arctic Snowpack Thaw Using the SeaWinds Scatterometer, *Journal of Hydrology*, 312: 294-311.

Rignot, E. and J.B. Way, 1994. Monitoring freeze-thaw cycles along North-South Alaskan transects using ERS-1 SAR, *Remote Sensing of Environment*, 49(2): 131-137.

Schaefer K, H. Lantuit, V.E. Romanovsky, E. Schuur, and R. Witt, 2014. The impact of the permafrost carbon feedback on global climate, *Environmental Research Letters*, 9(8): 085003.

Stocker, T.F., D. Qin, G.-K. Plattner, M. Tignor, S. K. Allen, J. Boschung, A. Nauels, Y. Xia, V. Bex and P.M. Midgley, 2013. *Summary for policymakers Climate Change 2013: The Physical Science Basis, the Contribution of Working Group I to the Fifth Assessment Report of the Intergovernmental Panel on Climate Change*, Cambridge University Press, Cambridge UK.

Way, J.B., R. Zimmermann, E. Rignot, K.C. McDonald, and R. Oren, 1997. Winter and spring thaw as observed with imaging radar at BOREAS, *Journal of Geophysical Research*, 102: 29673-29684.

Wisemann, V., 2000. Monitoring of seasonal thawing in Siberia with ERS scatterometer data, *IEEE Transactions on Geoscience and Remote Sensing*, 38(4): 1804-1809.

Yamaguchi, Y., Y. Yamamoto, H. Yamada, J. Yang, and W.-M. Boerner, 2008. Classification of terrain by implementing the correlation coefficient in the circular polarization basis using X-band POLSAR data, *IEICE Transactions on Communications*, 91(1): 297-301.